

## Interplanetary Signatures of Unipolar Streamers and the Origin of the Slow Solar Wind

P. Riley<sup>1</sup> · J. G. Luhmann<sup>2</sup>

© Springer ●●●●

**Abstract** Unipolar streamers (also known as pseudostreamers) are coronal structures that, at least in coronagraph images, and when viewed at the correct orientation, are often indistinguishable from dipolar (or “standard”) streamers. When interpreted with the aid of a coronal magnetic field model, however, they are shown to consist of a pair of loop arcades. Whereas dipolar streamers separate coronal holes of the opposite polarity and whose cusp is the origin of the heliospheric current sheet, unipolar streamers separate coronal holes of the same polarity and are therefore not associated with a current sheet. In this study, we investigate the interplanetary signatures of unipolar streamers. While it has been established that dipolar streamers are associated with the slow solar wind, we show that the two leading ideas concerning the origin of the slow solar wind suggest distinctly different wind properties from unipolar streamers. Specifically, the Expansion Factor (EF) model predicts fast solar wind from unipolar streamers, while the interchange reconnection (IR) model predicts slow wind. Using a global MHD model of the solar corona driven by the observed photospheric magnetic field, in combination with empirically-based implementations of the EF and IR models, we derive velocity profiles and compare them with ACE *in-situ* measurements for Carrington rotation 2060, during which time, ACE fortuitously traversed through a large, well-defined unipolar streamer. The results strongly suggest that the solar wind associated with unipolar streamers is slow, consistent with the IR model, but in apparent conflict with the EF model. Thus, our results suggest that: (1) slow (and dense) solar wind emanates from the boundary of any type of streamer structure; and (2) although associated with it, the expansion factor of coronal fields is not the principal parameter governing the speed of the solar wind.

**Keywords:** Sun, Corona, Evolution, Magnetic Fields, Solar Wind, Interplanetary Medium

---

<sup>1</sup> Predictive Science, Inc., 9990 Mesa Rim Road, Suite 170, San Diego, CA.

<sup>2</sup> Space Science Laboratory, University of California, Berkeley, Berkeley, CA.  
email: pete@predsci.com email: jgluhman@ssl.berkeley.edu

## 1. Introduction

The recent and prolonged solar minimum occurring at the end of solar cycle 23 (December, 2009) has provided a unique opportunity to investigate the Sun and its extended atmosphere (the heliosphere) under pristine, quiescent conditions. In contrast to the previous minimum (September, 1996) the structure of the corona was punctuated by the ubiquitous presence of “unipolar” helmet streamers (Hundhausen, 1972), also known as pseudo-streamers (Wang, Sheeley, and Rich, 2007). Whereas the standard helmet streamer, or “dipolar” streamer bridges between coronal holes of opposite polarity, unipolar streamers separate coronal holes of the same magnetic polarity. To accomplish this, two loops are embedded within them. Importantly, while dipolar streamers culminate in stalks with an embedded current sheet, no current sheet is embedded within unipolar streamers since the field lines on either side of the stalk have the same polarity. Figure 1 shows a selection of views for Carrington rotation (CR) 2060 illustrating the these principles. These views illustrate the general features of the solar corona surrounding this period. Simulated white light images, obtained by integrating the model density along the line of sight with an appropriate weighting function for electron scattering of light, are displayed together with a selection of field lines equally spaced in latitude. Closed field lines are colored green while open field lines that are directed away from the Sun are colored red and those directed toward the Sun are colored blue. A selection of dipolar and unipolar streamers are indicated, as is the latitude of the Ulysses and ACE spacecraft at these times. Although most of the unipolar streamers can be identified by the double loop structure under the streamer, note that the one in panel (c) cannot be resolved this way, at least on this scale. Instead, the closely-spaced field lines alerts us to its presence, suggesting a very small expansion factor.

Identifying and interpreting interplanetary signatures of phenomena observed in the corona can be challenging, complicated by the fact that the plasma undergoes significant evolution as it travels from the solar surface to 1 AU (or beyond). In the absence of obviously transient phenomena such as coronal mass ejecta, three quasi-corotating features in the solar wind are germane to this study: The stream interface (SI), the heliospheric current sheet (HCS), and the heliospheric plasma sheet (HPS), all of which have been associated with features or processes originating in the corona.

The SI is simply a boundary that separates what was originally slow and dense solar wind with what was fast, tenuous wind (Sonett and Colburn, 1965). Although this boundary can exist at the trailing edge of high-speed streams, that is, where fast solar wind outruns slower wind behind it, the term is usually used to refer to the leading edge of high-speed streams where fast wind runs into slower wind ahead, compressing and accelerating it (Gosling *et al.*, 1978).

The HCS is the extension of the neutral line in the corona identifying the boundary between outwardly-directed and inwardly-directed heliospheric magnetic field lines. Although its presence is often associated with SIs (Gosling *et al.*, 1978), with the HCS preceding the SI by a day or so, they are only loosely related, and, as we will see, during times when unipolar streamers are present (Wang, Sheeley, and Rich, 2007; Wang *et al.*, 2010), it is quite possible for SIs to exist in the absence of an HCS crossing.

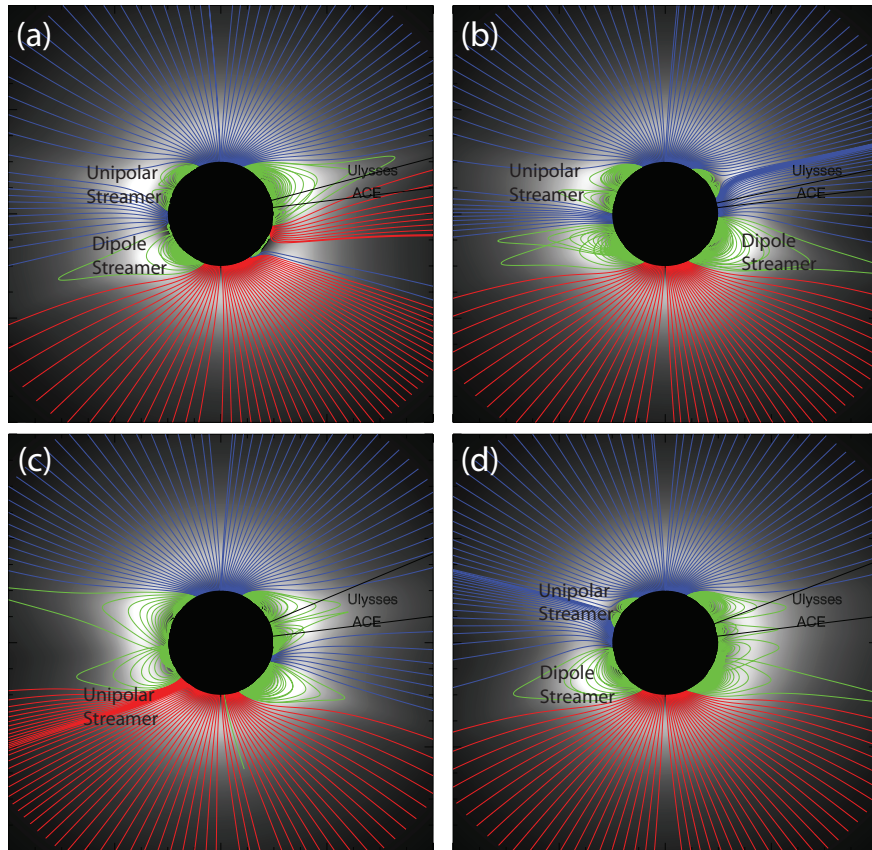


**Figure 1.** A selection of meridional slices from a global MHD simulation of CR 2060, which occurred between 08/14/2007 and 09/10/2007. Grey-scale images are Simulated polarized brightness (pB) images and the colored lines are magnetic field lines drawn from equally-spaced points in latitude on the solar surface. The field lines have been color-coded so that blue/red lines are field lines that open into the heliosphere and are inwardly/outwardly directed, while green field lines connect back to the Sun at both ends, i.e., they are closed field lines.

Finally, the HPS is a region surrounding the HCS of enhanced density but depressed magnetic field strength (Winterhalter *et al.*, 1994). Thus it is a region of significantly enhanced plasma  $\beta$ , where  $\beta$  is the ratio of thermal plasma pressure to magnetic pressure. Winterhalter *et al.* (1994) estimated the thickness of the HCS to be approximately 320,000 km, which is consistent with the superposed epoch analysis by Gosling *et al.* (1981), which also demonstrated that the HPS typically occur within regions of slow wind (that is, they are not associated with stream interactions). Gosling *et al.* (1981) mapped these events back to the Sun finding a strong association with coronal streamers. Thus, there is a strong connection between HCSs and HPSs, that is, the latter are almost always present when the former are observed (?). On the other hand, it is possible for HPSs to be observed in the absence of HCSs. Neugebauer *et al.* (2004), for example, identified consecutive fast solar wind streams of the same polarity. They found that the interaction region between the two had many of

the same features as intervals between streams that contained a sector boundary. In particular, quantities not expected to evolve with stream dynamics, such as helium abundances and heavy ion charge states, were not substantially different from their HCS-related counterparts. They did, however, find some differences in their dynamical properties: non-HCS regions were shorter in duration, had a higher minimum speed, and lower peak and mean densities. They found no obvious correlation between these intervals and coronal streamers.

The origin of the solar wind, and particularly the slow solar wind has remained elusive since the two basic properties of the wind were first measured in 1962 (Neugebauer and Snyder, 1962). While the fast solar wind is thought to originate from within coronal holes, we cannot point to a definitive location or basic physical mechanism for producing the slow solar wind. Although it has been long known that the slow, and variable solar wind is associated with the edges of coronal streamers (Gosling *et al.*, 1981), as yet, we have not been able to narrow it down further, at least in a way that the scientific community agrees upon. Two distinct ideas on its origin have arisen. (Of course, there are more models and even finer classifications of slow solar wind, but for simplicity, we limit our discussion to these two ideas). The first, which we will call the “expansion factor” (EF) model, relies on the geometrical properties of groups of the fields lines, or flux tubes as they expand into the heliosphere. In analogy with Bernoulli flow (and this is strictly an analogy - the Bernoulli effect is much too small to account for the difference in speed between the slow and fast wind), flow along flux tubes that expand the most leads to the slow solar wind, whereas flow along flux tubes that expand only modestly produce fast wind. It turns out that the expansion factor is smallest deep within coronal holes and largest adjacent to dipolar streamers (Wang and Sheeley, 1990). Crucially, however, because there is no current sheet to repel the field lines, the expansion factor associated with field lines near unipolar streamers is very small (sometimes as low as 1), leading to the prediction that solar wind from unipolar streamers will be fast (Wang, Sheeley, and Rich, 2007). Although the EF model was originally conceived because of an observed inverse correlation between expansion factor and measured solar wind speed at 1 AU, over the years, a theoretical basis for explaining how expansion factor can modulate not just speed, but density, composition, and charge state has been developed (Wang and Sheeley, 2003; Cranmer, van Ballegoijen, and Edgar, 2007; Wang, Ko, and Grappin, 2009; Cranmer, 2010).

A competing idea for the origin of the slow solar wind relies on the process of magnetic reconnection to open closed field lines within coronal streamers. A principal strength lies in its intrinsic ability to account for the difference in composition and abundance states of the slow and fast wind, which are sufficiently different that they imply distinct origins for slow and fast wind. Moreover, the composition and charge states measured in the slow wind are quite close to those measured within coronal streamers (e.g., Uzzo *et al.* (2003)). Since it is apparently necessary for an open magnetic field line to reconnect with one of the streamer loops, the term “interchange reconnection” has arisen to describe the way a closed field line opens while the open field line closes (e.g., Crooker *et al.* (2004)). We will generically refer to all incarnations of such models as interchange reconnection (IR) models, realizing that the concepts

behind them can be quite different (Wang, Hawley, and Sheeley Jr, 1996; Fisk, 1996; Antiochos *et al.*, 2010). The main point, however, is that the boundary between open and closed field lines provides an environment for reconnection to take place. And, in particular, it is not sensitive to whether there are one, two, or even three arcades underneath the streamer structure. We used a global MHD simulation to demonstrate how differential rotation could drive reconnection at the boundary of coronal streamers (Lionello *et al.*, 2005), substantiating the findings of Wang, Hawley, and Sheeley Jr (1996). Additionally, we showed that the regions where closed magnetic loops reconnect with open field lines may not be distributed uniformly along the boundaries of coronal holes; they are concentrated on the eastward borders of streamers, which may or may not be related to the studies by Suess *et al.* (2009) and Liu *et al.* (2010), who showed that tracers of composition (e.g., He/H, and  $O^{6+}/H$ ) are preferentially located to one side of the HCS.

Figure 2 illustrates the basic features and predictions of the EF and IR models for both dipolar (left) and unipolar (right) streamer geometries. For dipolar streamers, both models predict slow solar wind on either side of the HCS. The width of the slow-flow band is determined in the IR model by the details of where the reconnection is taking place, but is presumably limited to some distance away from the closed loops. The boundary of the slow-flow band in the EF model is determined by an interesting property of the time-independent Parker equations, namely, that for rapidly expanding flux tubes, there may be more than one location for the critical point, the most stable of which is that one furthest from the Sun (Cranmer, van Ballegoijen, and Edgar, 2007).

Figure 2(b) illustrates the situation for the case of a unipolar streamer. The concepts for the generation of slow solar wind under the IR model are unaltered: Reconnection still occurs between open and closed field lines. (Of course it remains to be demonstrated how reconnection can occur within a geometry where all field lines are apparently pointing in the same direction). However, the situation is fundamentally different under the EF picture. Here, field lines closest to the streamer effectively pile up on one another producing an expansion factor that can be as low as one. Under such conditions, the EF model would be expected to produce speeds even higher than in the fast solar wind ( $> 750\text{km s}^{-1}$ ).

The essence of both the IR and EF models have been implicitly incorporated into two empirically-based models for computing the speed of the solar wind in the heliosphere. (Of course, in reality, it could be argued that these empirically-based models preceded the theoretical ideas). First, the original Wang-Sheeley (WS) model (Wang and Sheeley, 1990) uses an observed negative correlation between solar wind speed and the super-radial expansion of the solar magnetic field. Second, PSI’s “Distance from the Coronal Hole Boundary” (DCHB) model (Riley *et al.*, 2001) specifies speed at the base of the corona as a function of the perpendicular distance from the coronal hole boundary and maps this speed out along field lines to  $30R_{\odot}$ . In effect, we consider a “boundary layer” adjacent to the last closed streamer field line that is where the reconnection takes place, opening up the streamer field lines.

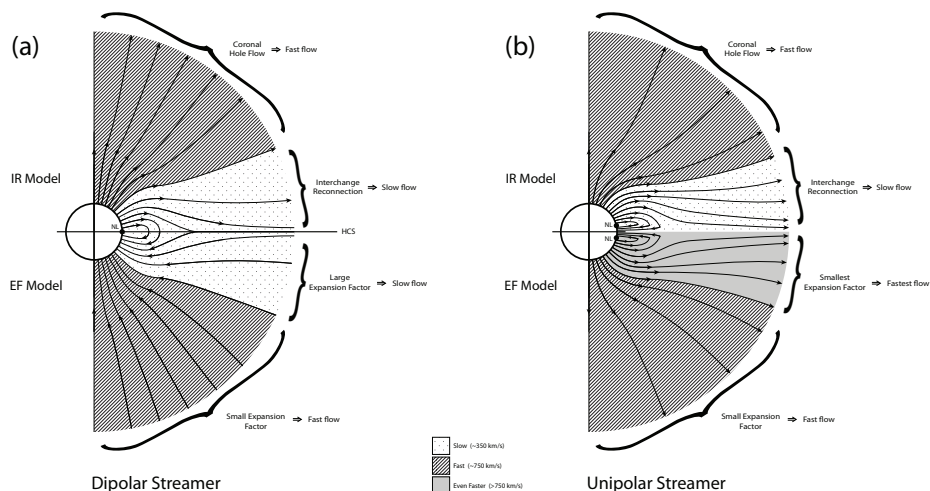


**Figure 2.** An illustration of the salient features of the EF and IR models for: (a) a dipolar streamer and (b) a unipolar streamer.

Although the derivation of solar wind speed at, say,  $30R_{\odot}$  in the WS and DCHB models is empirical (or “ad hoc”), the prescriptions are linked to fundamentally different ideas on the origin of the slow solar wind. Thus, in principle, it may be possible to derive some physical insight from comparisons of the two approaches. In the case of the WS model, which relies on the expansion factor of the local flux tube to govern the resulting speed, density, and temperature of the escaping solar wind, detailed physics-based models have been developed to produce the correct plasma properties driven by waves and turbulence (Cranmer, 2010), as well as the unique compositional differences between slow and fast solar wind (Laming, 2004). The DCHB model, on the other hand, which linked to the idea of “interchange reconnection” for the origin of the slow solar wind (Fisk, 1996; Antiochos *et al.*, 2010) provides a natural explanation for the composition and charge state distributions in the slow solar wind, as well as speed, density, and temperature, at least in a qualitative sense. Thus, should the WS or DCHB models perform significantly better than the other, this would provide support for either the EF or IR model, respectively. Of course, this would remain a tentative conclusion until comprehensive statistical studies confirmed the result.

In their original paper, Wang and Sheeley (1990) determined a relationship between solar wind speed ( $V$ ) and expansion factor ( $f_s$ ) using very broad velocity bins of size  $\Delta v = 100 \text{ km s}^{-1}$  applied to solar wind data between  $450 \text{ km s}^{-1}$  and  $750 \text{ km s}^{-1}$  (a bin on either end collected all speeds outside this range). Here, following and generalizing Arge and Pizzo (2000) we write a continuous form of relationship between solar wind speed and expansion factor:

$$V_{WS}(f_s) = V_{slow} + \frac{V_{fast}}{(f_s)^{\delta}} \quad (1)$$

where  $f_s v_{slow}$  is the lowest solar wind speed expected as  $f_s \rightarrow \infty$  and  $\alpha$  is some coefficient also to be determined, although Wang (Personal Communication, 2010) suggests that  $\delta = 1$  is justified. The specification of velocity then depends only on the expansion factor of the field line.

Using values from Wang and Sheeley (1990), we performed a least-squares fit to derive  $V_{slow} = 377.5 \text{ km s}^{-1}$  and  $V_{fast} = 1863 \text{ km s}^{-1}$ . Since this expression can potentially lead to speeds well beyond those that have been observed by Ulysses, we also impose a minimum and maximum speed of 350, and 800  $\text{km s}^{-1}$ . These values could also be considered free parameters. Although Arge (2004) derived set of best-fit parameters (which are sensitive to the solar observatory used to create the photospheric field map), the precise values of these parameters are not that important for the current study, and for simplicity, we retain the parameters originally derived in the Wang and Sheeley (1990) study.

The ‘‘Distance from the Coronal Hole Boundary’’ (DCHB) model depends on the angular, minimum (perpendicular) distance from the coronal hole boundary to specify solar wind speed. This is computed at the base of the corona and the speeds are mapped along field lines to the reference sphere,  $30R_\odot$ , in this case. We can express the relationship as:

$$V_{DCHB}(d) = V_{slow} + \frac{1}{2}(V_{fast} - V_{slow}) \left( 1 + \tanh \left( \frac{d - \alpha}{w} \right) \right) \quad (2)$$

where  $d$  is the minimum, or perpendicular distance from an open-closed boundary, that is from a CH boundary, at the base of the corona,  $\alpha$  is a measure of how thick the slow flow band is, and  $w$  is the width over which the flow is raised to coronal hole values (Riley, Linker, and Mikić, 2001). The parameters  $V_{slow}$  and  $V_{fast}$  are analogues (but, because of the difference in formulation, likely to be different) of the same-named parameters in the WS model. At the boundary between open-closed fields, this expression reduces to  $v_{slow}$ , whereas, far from such a boundary, that is, deep within a coronal hole, it reduces to  $v_{fast}$ . For the DCHB model, then, the specification of the velocity profile depends on the minimum distance of the field line foot-point to a coronal hole boundary.

It is important to distinguish the DCHB model from an earlier prescription based on the minimum angular distance from the heliospheric current sheet (Hakamada and Akasofu, 1981). In the latter, the wind speed is assumed to be slow in a band within some angular minimum distance from the heliospheric current sheet, computed at some reference height (say  $2.5R_\odot$  for PFSS models or  $20 - 30R_\odot$  for MHD models) and fast everywhere else. On the other hand, the DCHB model specifies the slow wind along bands at the base of the corona, adjacent to the open-closed field line boundaries. This speed profile is then mapped along field lines to some reference height. Except for very idealized geometries, such as a tilted dipole field, these would be expected to yield quite different results. The DCHB model attempts to describe the wind profile near its source, whereas the technique based on distance from the HCS attempts to describe the profile at some point of relative equilibrium. Wang and Sheeley (1997) compared the WS and angular distance from the HCS models finding that the latter produced significantly poorer correlations with *in-situ* measurements at Earth.

Finally, it is worth noting that a third empirically-based model exists, which is, arguably, the most well known and implemented. The Wang-Sheeley-Arge (WSA) has been successively refined since its initial development in the late 1990's at NOAA's Space Weather Prediction Center (SWPC) and was recently a key component in the first research model transitioned to space weather operations (Farrell, 2011). Initially, it developed via a set of minor adjustments to the WS model, tuning the free parameters using more thorough comparisons with *in-situ* observations. More recently, the relationship between speed and  $f_s$  was been generalized, and a term similar to that in the DCHB model was also been added (Arge, Personal Communication, 2010). In fact, in its current form, the best-fit parameters for the WSA model render it virtually identical to the DCHB model. Ironically, we believe that the residual effects of the WS model in the WSA model serve only to reduce its ability to match solar wind streams (Riley *et al.*, 2011).

## 2. Unipolar Streamers in the Corona

We begin our analysis by summarizing the structure of the solar corona during the interval between 08/14/2007 and 09/10/2007, that is, CR 2060. We chose this time period for our case study for several reasons. First, it is one of the more quiescent rotations during the interval spanning the last solar minimum (marking the end of solar cycle 23), and there were no obvious signatures of transient activity during the interval. Second, well-developed unipolar streamers were observed (see Figure 1). And third, and most importantly, the ACE spacecraft, located at  $7.1^\circ$  N latitude was positioned such that its trajectory took it directly through plasma emanating from one of the unipolar streamers.

To assess how well our MHD model has reproduced the large-scale streamer structure during CR 2060, in Figure 3 we compare our simulated polarized brightness estimates with brightness observations by the SECCHI instruments on board STEREO. The particular combination of STEREO A/B and COR1/2 images were selected from the full set available at <http://secchi.nrl.mil/synomaps> based on the quality of the images. At least for this rotation, we found that the combination of COR1 from STEREO B at lower altitudes and COR2 from STEREO A at higher altitudes resulted in the best set. Since the model used here relied on the polytropic approximation, we are limited to a qualitative assessment of model results. In spite of this, the comparison demonstrates that the model has captured the overall features of the streamer structure existing during CR 2060. In particular, we note the following: (1) There is a dominant streamer pattern tracing through all longitudes that first rises into the northern hemisphere, drops across the equator at  $\sim 180^\circ$  and finally returns to the northern hemisphere. As we will show later, this pattern tracks the location of the HCS as determined from the model.

## 3. Solar Wind Speed from Unipolar Streamers

The stream structure of the solar wind at 1 AU in the ecliptic plane (from ACE measurements) is shown in the bottom panel of Figure 4 (bottom panel). We have

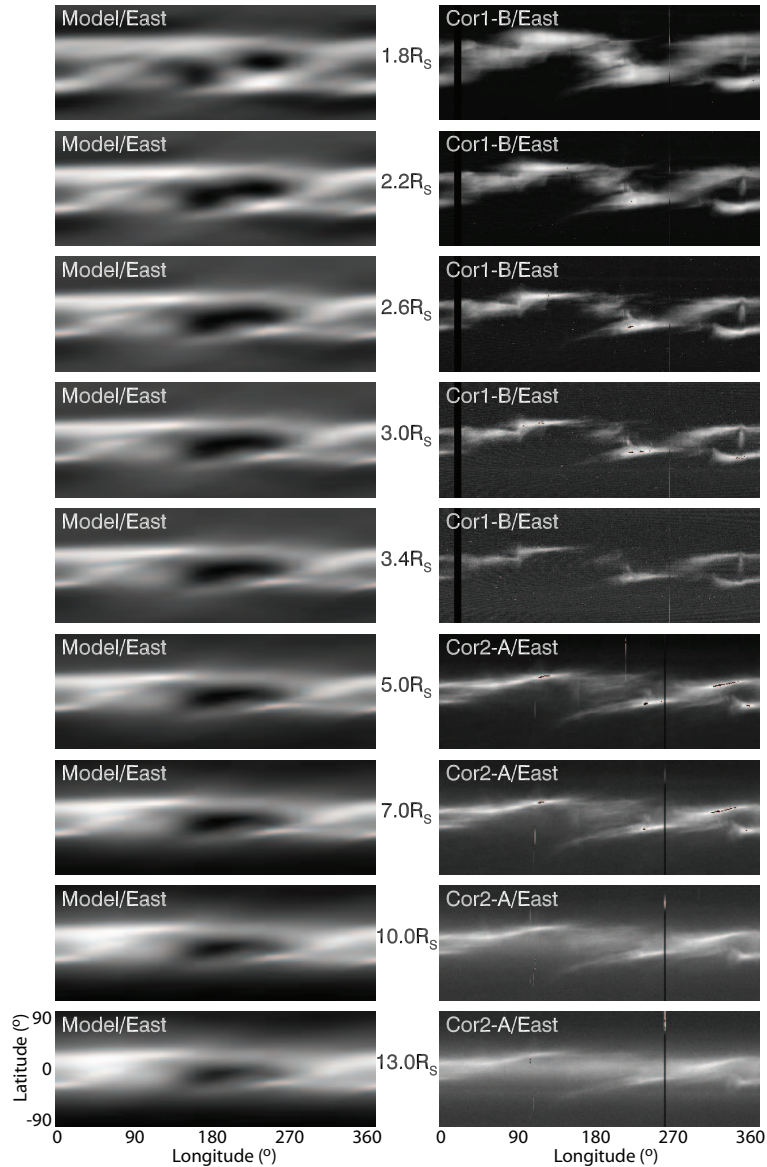


**Figure 3.** Comparison of model results with white light synoptic maps from COR1 and COR2 instruments on board STEREO A and B spacecraft. The images were assembled from east limb observations and have been arbitrarily scaled to bring out the structure contained within each.

plotted both solar wind speed, color-coded according to the observed polarity of the interplanetary magnetic field, together with plasma density (green) as a function of Carrington longitude, ballistically-mapped back from 1 AU to the Sun. In this presentation of the data, time increases from right to left. Thus, a fast stream will evolve - as it moves away from the Sun - by steepening at

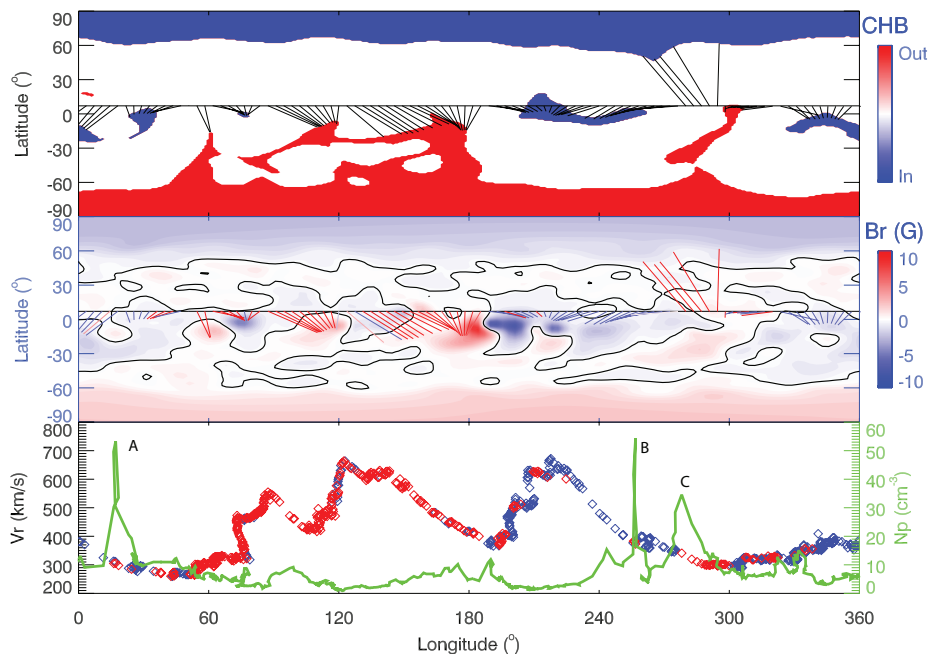


**Figure 4.** (Top) Coronal holes for CR 2060 computed from the MHD solution and color-coded according to the observed underlying photospheric magnetic field. The trajectory of the ACE spacecraft is superimposed, together with the mapped source regions of the plasma measured at ACE. (Middle) Photospheric magnetic field (color contours), location of the neutral line (black line), and mapped source regions of ACE measurements color-coded according to the observed *in-situ* polarity of the magnetic field embedded in the plasma. (Bottom) Ballistically-mapped ACE speed (red/blue) and plasma density (green). The speed has been color-coded according to the measured polarity of the *in-situ* magnetic field.

its leading (right) edge and becoming shallower at its trailing (left) edge. The former lead to compression fronts, while the latter produce expansion waves, or rarefaction regions (Sarabhai, 1963). The density enhancement at  $\sim 255^\circ$  longitude (labeled ‘A’) likely marks the location of a SI, separating fast wind to its left from slow wind to its right. The pattern within the magnetic polarity of the flow is, to a first approximation, two-sector, with the first half of the interval being outward (red) magnetic field and the second half being inward (blue). It is, however, more complex, with “pockets” of opposite polarity embedded within the larger scale pattern.

The middle and top panels of Figure 4 indicate where the ACE observations map back to on the surface of the Sun, using the MHD solution. To accomplish this, the trajectory was ballistically mapped back to  $30R_\odot$ , after which the MHD solution was then used to trace along field lines to their source at the base of the corona. In the middle panel, the red and blue lines show where points on the ACE trajectory map to at the base of the corona. The color-coding is based on the polarity of the interplanetary magnetic field, as measured by ACE. The color contours show the observed photospheric magnetic field, while the black contours mark the neutral line, that is, where  $B_r = 0$ . Finally, the ACE trajectory and

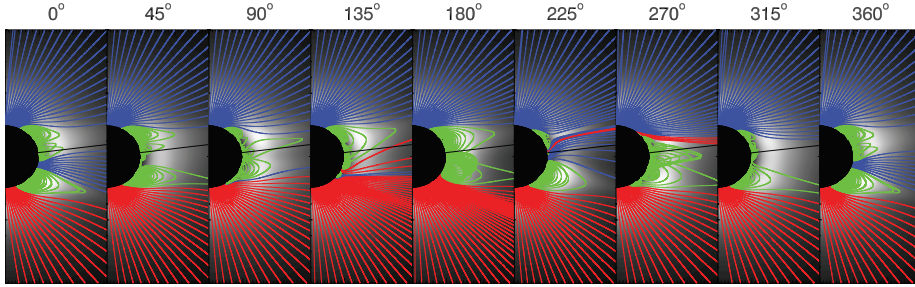


**Figure 5.** (Top) Selection of meridional slices of pB with field lines superimposed, equally spaced in longitude. Field lines colored blue (red) open into the heliosphere and are inward (outward), while field lines drawn in green are closed. The solid black line indicates the latitude of the ACE spacecraft during this interval.

mapping is overlaid on the computed coronal holes for this solution, color-coded by the direction of the photospheric field.

Comparing the mapped ACE polarities with the observed photospheric field (middle panel) suggests a reasonable match between the two. There are some obvious disagreements, such as the outward IMF mapping into the northern polar coronal hole around longitudes  $280 - 300^\circ$ , but overall, the large-scale polarity appears to trace back correctly. Where the comparison is poor, it could suggest: (1) there are inaccuracies in the model solution - computed coronal holes are larger/smaller than in reality, for example; or (2) there were processes not incorporated in the model, such as long period Alfvén waves, turbulence, or transient activity.

Returning to the bottom panel of Figure 4, we can interpret the interval between the first-two streams ( $\sim 105^\circ$  longitude) as a non-HCS interaction region (Neugebauer *et al.*, 2004), whereas the second trough, at  $\sim 200^\circ$  longitude contains an embedded HCS. Moreover, the first two streams likely originate from the midlatitude extension of the southern polar coronal hole, whereas the boundary between the second and third streams separates distinct locations (the southern extension and an equatorial coronal hole at  $\sim 240^\circ$  longitude. Finally, if we assume that the boundary between  $360^\circ$  and  $0^\circ$  longitude is periodic, that is, that the large-scale structure from 2059 through 2061 did not change appreciably, then the slow and essentially mono-polarity wind from  $300^\circ$  through  $40^\circ$  contains plasma from two distinct equatorial coronal holes, both with negative polarity.

In Figure 5, we have computed polarized brightness (pB) and overlaid field lines at a selection of Carrington longitudes. Field lines colored red/blue are open and directed outward/inward. Field lines that are colored green are closed, that is, they attach back to the Sun at both ends. Also shown is the latitude of the ACE spacecraft, which changed only modestly during the 25.38 days. These frames roughly match with the x-axis in Figure 4. We can identify two clear unipolar structures. First during the last  $30^\circ$  and first  $30^\circ$  of the rotation, a large unipolar streamer is present off the northwest limb. A much more compact unipolar streamer is also seen at  $\sim 225^\circ$ . Based on ACE's latitude during this interval, we can infer that it missed the compact unipolar streamer but likely sampled and spent a significant amount of time within the major one. In fact, it

is possible that the density enhancement labeled ‘A’ in Figure 4(bottom panel) is a direct measurement of the HPC associated with this unipolar streamer. In contrast, the density enhancement labeled ‘B’ is more likely a signature of the SI, separating the fast stream to the left from the slow stream to the right. Finally, event ‘C’ is probably a crossing of the HCS embedded within a HPS.

#### 4. Solar Wind Speed from Unipolar Streamers

Armed with an understanding of the basic stream structure measured by ACE and its likely connectivity with structure back at the Sun, we turn our attention to the question of what the WS and DCHB models predict for the structure of the solar wind at Earth during this time period. Panels (a) and (b) in Figure 6 compare velocity maps at  $30R_{\odot}$  computed from the WS and DCHB prescriptions. Several points are readily apparent. First, both models match at latitudes away from the “band of solar wind variability,” that is, from deep within the polar coronal holes. Second, following the trace of the HCS (white line in (a) and black line in (b)), both models predict slow solar wind. However, the band over which this slow wind exists is extremely thin ( $\sim \pm 1^{\circ}$  for the WS model. In contrast, the HCS-associated band in the DCHB model is  $\sim \pm 10^{\circ}$ . Third, where the two models differ most significantly is at the “conjugate” latitudinal point, that is, a trace in longitude that very roughly follows the negative value of the HCS. Of particular note is the spur branching off from the HCS at  $200^{\circ}$  longitude in the northern hemisphere and merging back into the vicinity of the HCS at  $\sim 300^{\circ}$ . Whereas in the DCHB model this is a flow region flanking faster flow from a coronal hole, in the WS model, the spur consists of wind traveling even faster than flow from deep within polar coronal holes. Importantly, and fortuitously, this spur is positioned such that ACE became immersed within it by  $\sim 240^{\circ}$ .

The ACE trajectory through these velocity profiles have been extracted and compared with ACE *in-situ* measurements in panels (c) and (d) of Figure 6. In panel (c), the ACE data has been ballistically-mapped back to  $30R_{\odot}$  to compare with the model results. In panel (d), the model results have been mapped from the Sun to 1 AU using the technique described by Riley *et al.* (2011).

Thus, the two comparisons in (c) and (d) are both limited in that there are assumptions in taking one dataset in or out to the location of the other. However, with this in mind, both views are also useful for interpreting the data, and the differences between the comparisons can be used to estimate the potential errors introduced by each mapping technique. Note further that the streams migrate to the left from  $30R_{\odot}$  to 1 AU, since we are using Carrington coordinates. Here, we focus on the high-speed stream centered at  $\sim 220^{\circ}$  in panel (c) or  $\sim 180^{\circ}$  in panel (d), and the remaining portion of the interval. While both the WS and DCHB models reproduce the basic structure of this stream (and the earlier one to the left), they differ significantly in their prediction of the wind following it. The WS model, as we have shown, predicts extremely fast wind from unipolar streamer regions, in which the spacecraft was immersed in during this interval. Notwithstanding any errors or optimizations that could be performed on the

WS technique, it's basic prediction is for fast wind to originate from the slowly expanding field lines surrounding unipolar streamers (Wang, Sheeley, and Rich, 2007; Wang *et al.*, 2010). On the other hand, and by construction, the DCHB predicts slow (and dense) solar wind emanates from the boundary of any type of streamer structure. Comparison with ACE measurements suggest a prolonged interval of slow solar wind, consistent with the predictions of the DCHB model.

A further point worth noting from Figure 6 is the richness in the variability of the slow-flow band. Considering the smoothing and filtering of the input magnetogram, it is quite remarkable that such complexity is produced. Of course, both because the solar wind tends to dampen out higher-frequency perturbations preferentially, and because the numerics of the code tend to do the same (through numerical diffusion), much of this structure is lost by 1 AU. It would be interesting to assess whether some or all of this fine-scale structure is real. As models become ever more capable of simulating smaller-scale phenomena, the computed results should retain more and more of this texture.

Finally, in Figure 7 we summarize solar wind speed, number density, proton temperature, and magnetic field strength for Carrington rotation 2060. Unfortunately, composition and charge state data during this interval was not available through the level 2 data products at the Ace Science Center. Two of the density enhancements from Figure 6 are also identified. Enhancement B, which showed a sharp rise of about one order of magnitude coincided with an abrupt drop in speed from the fast stream at  $\sim 180^\circ$  from the slower wind ahead. It is also coincident with a peak in magnetic field strength and a discontinuous drop in speed, signatures that are all consistent with an SI. The polarity of the field remains inward throughout the period surrounding enhancement B. In contrast, the density enhancement C is apparently associated with an albeit brief polarity change from inward to outward (with increasing longitude), but no significant change in speed. We suggest that this event is a crossing of the HPS and that there is a HCS embedded within it.

## 5. Summary and Discussion

In this study, we have used ACE *in-situ* measurements, in conjunction with a global MHD model of the solar wind to test a distinguishing prediction between two ideas for the origin of the slow solar wind. Specifically, models relying on the expansion factor of the coronal field lines predict that solar wind originating from unipolar (pseudo) streamers should be fast; even faster than wind originating deep within well-established, large polar coronal holes. In contrast, interchange reconnection models predict that wind originating from the boundary between open and closed field lines, regardless of whether the underlying loop structure produces unipolar or dipolar streamers, should be slow. Our comparison of model results with observations occurred during a serendipitous interval when: (1) there was no obvious transient activity; (2) well-developed unipolar streamers were present; and (3) ACE was positioned in latitude such that it could sample unipolar streamer wind directly. Our results strongly suggest that wind from unipolar streamers is slow, which is consistent with the basic premise of the IR model, but in conflict with the EF model.

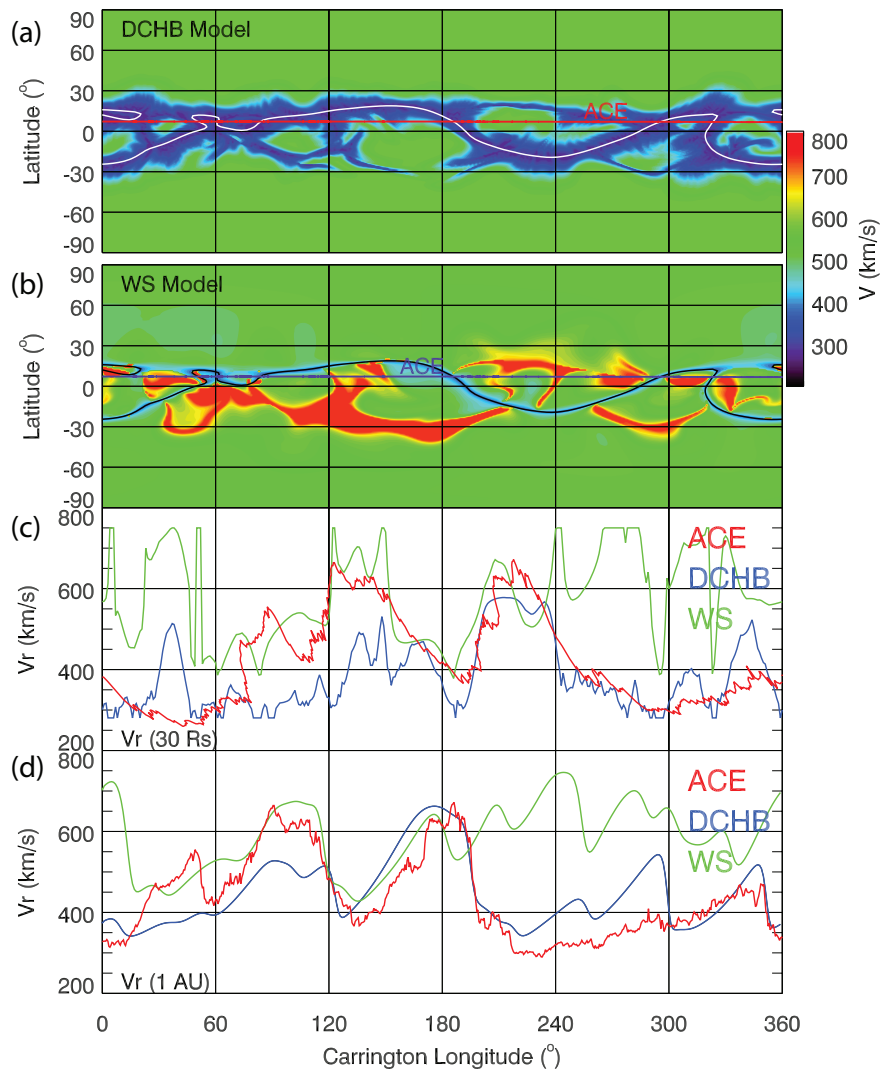


**Figure 6.** (a) Solar wind speed map at  $30R_{\odot}$  produced by the DCHB model. Superimposed are: (1) The HCS (white curve); and (2) the trajectory of the ACE spacecraft (red). (b) Solar wind speed map at  $30R_{\odot}$  produced from the WS model. The HCS and ACE trajectory as also shown as black traces. (c) Solar wind speed at  $30R_{\odot}$  as determined from: (1) ballistically mapping ACE in-situ measurements back from 1 AU (red); (2) extracting from the DCHB model (blue); and (3) extracting from the WS model (green). (d) Solar wind speed at 1 AU. Both the DCHB and WS model results were ‘evolved’ using the technique described by Riley *et al.* (2011).

Our results are in apparent disagreement with several aspects of the studies by Wang and colleagues. Wang, Sheeley, and Rich (2007) identified outflowing material, which they associated with a unipolar streamer, that was traveling at  $\sim 200\text{km s}^{-1}$  at  $\sim 3R_{\odot}$ . By comparison, similar profiles from within dipolar streamers during the same interval showed speeds of  $\sim 100\text{km s}^{-1}$  at the same

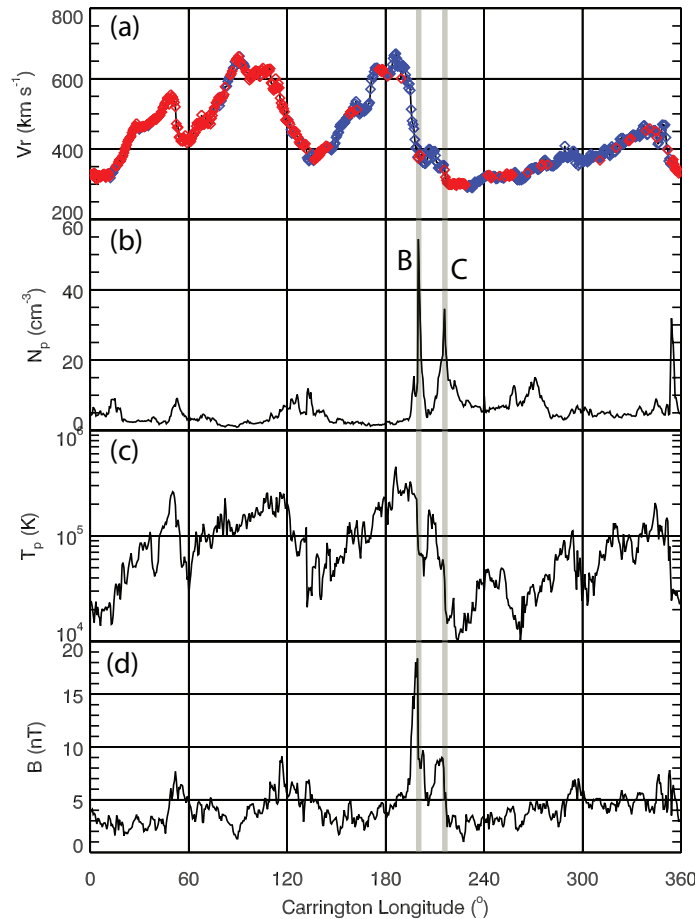


**Figure 7.** (a) Solar wind speed; (b) number density; (c) proton temperature; and (d) magnetic field strength as a function of Carrington longitude (at 1 AU) for Carrington rotation 2060. Two density enhancements are labeled ‘B’ and ‘C’ and discussed in more detail in the text.

distance. However, this assumes that the outflows being measured are, in fact, fiduciaries of the ambient solar wind flow. Sheeley *et al.* (1997) has argued that these blobs are swept along “like leaves” by the ambient flow. Nevertheless, it is quite possible that they are propagating either faster or slower than the underlying quiescent flow.

Wang *et al.* (2010) identified what they claimed to be signatures of unipolar streamers in ACE *in-situ* measurements. One such case is event B in Figure 7. They argued that the high-density enhancement was a crossing of the HPS associated with the interplanetary extension of the unipolar streamer stalk. However, we have interpreted this, and other events identified by Wang *et al.* (2010) as SIs. Gosling *et al.* (1978) showed that SIs are interfaces that separate flow that was originally hot, tenuous, and fast with flow that was cooler, denser, and slower. Without exception, the events identified by Wang *et al.* (2010) occurred at the leading edges of high-speed streams, which would be expected to compress the

plasma producing the density enhancement observed. Moreover, we believe the event labeled B in Figure 7, which occurred  $\sim 15^\circ$  further in longitude, or  $\sim 1.1$  days preceding the SI is the HPS, and, the change in polarity coincident with it suggests that a current sheet was also crossed.

Our comparison between WS-derived speeds and 1 AU observations do not invalidate the results of Wang and colleagues (Wang and Sheeley, 1990; Wang, 1994; Wang *et al.*, 1997, 2010). Their comparisons are on such a large temporal scale (a single Figure in their studies may include more than 30 years of data) that the patterns being matched represent only the grossest features of the system. Whether they predict the correct phase of even the existence of a specific high-speed stream within a single Carrington rotation cannot be determined. The WS model does predict the appearance of slow solar wind in the vicinity of the HCS, i.e., associated with dipolar streamers, and thus, in the absence of unipolar streamers, it should be able to track the basic features of the slow solar wind. It is only because of the appearance of unipolar streamers in the recent solar minimum that the WS model appears to fail.

In closing, it is worth noting that our ability to differentiate between the two models (WS and DCHB, representing the EF and IR ideas) based on the presence of unipolar streamer structure was facilitated by the unique properties of the current minimum. Our conclusions are based on a careful analysis of a single Carrington rotation. To substantiate them now requires a systematic statistical analysis of coronal stream structure and *in-situ* measurements both during the recent minimum and contrasting it with structure from the earlier one (September, 1996). Ultimately, these comparisons should lead to better-constrained empirical models of the ambient solar wind structure in the vicinity of Earth, and, hopefully, provide key constraints for theories of the origin of the slow solar wind.

**Acknowledgements** PR gratefully acknowledges the support of NASA's Causes and Consequences of the Minimum of Solar Cycle 24 program, the LWS Strategic Capabilities Program (NASA, NSF, and AFOSR), the NSF Center for Integrated Space Weather Modeling (CISM), and NASA's Heliophysics Theory Program (HTP).

## References

- Antiochos, S.K., Mikić, Z., Lionello, R., Titov, V., Linker, J.A.: 2010, A model for the sources of the slow solar wind. *submitted to Ap. J.*
- Arge, C.N.: 2004, Working with the photospheric magnetic field observations from Mount Wilson, Wilcox, and Kitt Solar Observatories. *AGU Fall Meeting Abstracts*, A2.
- Arge, C.N., Pizzo, V.J.: 2000, Improvement in the prediction of solar wind conditions using near-real time solar magnetic field updates. *J. Geophys. Res.* **105**, 10465.

- Cranmer, S.R.: 2010, An Efficient Approximation of the Coronal Heating Rate for use in Global Sun-Heliosphere Simulations. *Astrophys. J. Lett.* **710**, 676–688. doi:10.1088/0004-637X/710/1/676.
- Cranmer, S.R., van Ballegoijen, A.A., Edgar, R.J.: 2007, Self-consistent Coronal Heating and Solar Wind Acceleration from Anisotropic Magnetohydrodynamic Turbulence. *Astrophys. J. Suppl. Ser.* **171**, 520–551. doi:10.1086/518001.
- Crooker, N.U., Kahler, S.W., Larson, D.E., Lin, R.P.: 2004, Large-scale magnetic field inversions at sector boundaries. *J. Geophys. Res.* **109**, 3108. doi:10.1029/2003JA010278.
- Farrell, P.: 2011, New Space Weather Forecasting Model Going Operational with National Weather Service. <http://www.bu.edu/cas/news/press-releases/cism/>.
- Fisk, L.: 1996, Motion of the footpoints of heliospheric magnetic field lines at the sun: Implications for recurrent energetic particle events at high heliographic latitudes. *J. Geophys. Res.* **101**(A7), 15547.
- Gosling, J.T., Asbridge, J.R., Bame, S.J., Feldman, W.C.: 1978, Solar wind stream interfaces. *J. Geophys. Res.* **83**, 1401.
- Gosling, J.T., Asbridge, J.R., Bame, S.J., Feldman, W.C., Borrini, G., Hansen, R.T.: 1981, Coronal streamers in the solar wind at 1 AU. *J. Geophys. Res.* **86**, 5438–5448. doi:10.1029/JA086iA07p05438.
- Hakamada, K., Akasofu, S.: 1981, A cause of solar wind speed variations observed at 1 A.U. *J. Geophys. Res.* **86**, 1290–1298. doi:10.1029/JA086iA03p01290.
- Hundhausen, A.J.: 1972, *Coronal Expansion and Solar Wind*.
- Laming, J.M.: 2004, On Collisionless Electron-Ion Temperature Equilibration in the Fast Solar Wind. *Ap. J.* **604**, 874–883. doi:10.1086/382066.
- Lionello, R., Riley, P., Linker, J.A., Mikić, Z.: 2005, The Effects of Differential Rotation on the Magnetic Structure of the Solar Corona: Magnetohydrodynamic Simulations. *Ap. J.* **625**, 463–473. doi:10.1086/429268.
- Liu, Y.C.M., Galvin, A.B., Popecki, M.A., Simunac, K.D.C., Kistler, L., Farrugia, C., Lee, M.A., Klecker, B., Bochsler, P., Luhmann, J.L., Jian, L.K., Moebius, E., Wimmer-Schweingruber, R., Wurz, P.: 2010, Proton Enhancement and Decreased  $O^{6+}/H$  at the Heliospheric Current Sheet: Implications for the Origin of Slow Solar Wind. *Twelfth International Solar Wind Conference* **1216**, 363–366. doi:10.1063/1.3395875.
- Neugebauer, M., Snyder, C.W.: 1962, Solar Plasma Experiment. *Science* **138**, 1095–1097. doi:10.1126/science.138.3545.1095-a.

- Neugebauer, M., Liewer, P.C., Goldstein, B.E., Zhou, X., Steinberg, J.T.: 2004, Solar wind stream interaction regions without sector boundaries. *J. Geophys. Res.* **109**, 10102. doi:10.1029/2004JA010456.
- Riley, P., Linker, J.A., Mikić, Z.: 2001, An empirically-driven global mhd model of the corona and inner heliosphere. *J. Geophys. Res.* **106**, 15889.
- Riley, P., Lionello, R., Linker, J.A., Mikic, Z., Luhmann, J., Wijaya, J.: 2011, Global MHD Modeling of the Solar Corona and Inner Heliosphere for the Whole Heliosphere Interval. *Solar Phys.*, in press.
- Sarabhai, V.: 1963, Some consequences of nonuniformity of solar wind velocity. *J. Geophys. Res.* **68**, 1555.
- Sheeley, N.R. Jr., Wang, Y.M., Hawley, S.H., Brueckner, G.E., Dere, K.P., Howard, R.A., Koomen, M.J., Korendyke, C.M., Michels, D.J., Paswaters, S.E., Socker, D.G., St. Cyr, O.C., Wang, D., Lamy, P.L., Llebaria, A., Schwenn, R., Simnett, G.M., Plunkett, S., Biesecker, D.A.: 1997, Measurements of Flow Speeds in the Corona between 2 and 30 R sub sun. *Ap. J.* **484**, 472. doi:10.1086/304338.
- Sonett, C.P., Colburn, D.S.: 1965, The SI+-Si- pair and interplanetary forward-reverse shock ensembles. *Plan. Space. Sci.* **13**, 675. doi:10.1016/0032-0633(65)90046-2.
- Suess, S.T., Ko, Y.K., von Steiger, R., Moore, R.L.: 2009, Quiescent current sheets in the solar wind and origins of slow wind. *J. Geophys. Res.* **114**, A04103. doi:10.1029/2008JA013704.
- Uzzo, M., Ko, Y.K., Raymond, J.C., Wurz, P., Ipavich, F.M.: 2003, Elemental Abundances for the 1996 Streamer Belt. *Ap. J.* **585**, 1062–1072. doi:10.1086/346132.
- Wang, Y.M.: 1994, Two types of slow solar wind. *Ap. J. Lett.* **437**, L67–L70. doi:10.1086/187684.
- Wang, Y.M., Sheeley, J. N. R.: 1997, The high-latitude solar wind near sunspot maximum. *Geophys. Res. Lett.* **24**(24), 3141.
- Wang, Y.M., Sheeley, N.R. Jr.: 1990, Solar wind speed and coronal flux-tube expansion. *Astrophys. J.* **355**, 726.
- Wang, Y.M., Sheeley, N.R. Jr.: 2003, The Solar Wind and Its Magnetic Sources at Sunspot Maximum. *Ap. J.* **587**, 818–822. doi:10.1086/368302.
- Wang, Y.M., Hawley, S.H., Sheeley Jr, N.R.: 1996, The magnetic nature of coronal holes. *Science* **271**, 464.
- Wang, Y., Ko, Y., Grappin, R.: 2009, Slow Solar Wind from Open Regions with Strong Low-Coronal Heating. *Ap. J.* **691**, 760–769. doi:10.1088/0004-637X/691/1/760.

- Wang, Y.M., Sheeley, N.R. Jr., Rich, N.B.: 2007, Coronal Pseudostreamers. *Astrophys. J.* **658**, 1340–1348. doi:10.1086/511416.
- Wang, Y.M., Sheeley, N.R. Jr., Phillips, J.L., Goldstein, B.E.: 1997, Solar Wind Stream Interactions and the Wind Speed-Expansion Factor Relationship. *Ap. J. Lett.* **488**, L51. doi:10.1086/310918.
- Wang, Y.M., Robbrecht, E., Rouillard, A.P., Sheeley, N.R., Thernisien, A.F.R.: 2010, Formation and Evolution of Coronal Holes Following the Emergence of Active Regions. *Ap. J.* **715**, 39–50. doi:10.1088/0004-637X/715/1/39.
- Winterhalter, D., Smith, E.J., Burton, M.E., Murphy, N., McComas, D.J.: 1994, The heliospheric plasma sheet. *J. Geophys. Res.* **99**, 6667–6680. doi:10.1029/93JA03481.

